

REALTIME FAILURE FORECASTING FOR FLAT, BALL-NOSE, ROUGHING, AND TAPERED ENDMILLS USING AN ACCELEROMETER

**Christopher A. Suprock and John T. Roth
School of Engineering, Mechanical Engineering
Penn State Erie, The Behrend College
Erie, PA**

**Larry M. Downey
School of Science, Mathematics
Penn State Erie, The Behrend College
Erie, PA**

KEYWORDS

Wear, Endmill, Ball-nose, Roughing, Tapered

ABSTRACT

In this paper, flat, ball-nose, roughing, and tapered endmilling tools are investigated for their respective wear trends. These curves are contrasted with the trend exhibited by traditional flat endmills. To isolate the wear behavior of the various tool geometries, an autoregressive based monitoring algorithm is used to track the tool's condition using a tri-axial accelerometer. An accelerometer is used due to its low cost and since it does not limit the machining envelope. To demonstrate repeatability, eight life tests were conducted (two life tests for each type of endmill). The technique discussed herein successfully identifies impending fracture or meltdown due to wear in all cases, providing sufficient time to remove the tools before failure is realized. Furthermore, the algorithm produces similar trends capable of forecasting failure, regardless of tool geometry, in all cases, without requiring algorithm modifications or a priori information regarding the cutting conditions.

INTRODUCTION

When machining a part, milling tools of various geometric configurations are frequently used to achieve a desired profile or surface finish. Therefore, to automate cutting operations, it is vital for tool condition monitoring techniques to be developed that track a tool's condition for various geometries. In recent years, many methods have been proposed for monitoring the tool condition of a specific endmilling geometry (i.e, flat, ball, etc.). For instance, the algorithm developed by Chen and Chen (2005) studies flat tools, whereas the investigations by Ning and Veldhuis (2004), Rodriguez and Altan (2000), and Azeem et al. (2003) all focused on monitoring ball nose endmills. When monitoring the tool's condition, numerous approaches exist. In work by Ko and Cho (2002) the possibility of error compensation using geometry condition monitoring was investigated. Also, applications of tool condition monitoring such as process optimization were studied by Xu et al. (2006). Similarly, Choi and Chung (2006) utilize machine vision to determine when the tool needs to be changed when micro-drilling. Olortegui-Yume and Kwon (2006) uses wear monitoring to show benefits associated with particular coatings. Tool condition monitoring

algorithms for flat endmills have also been discussed in the works by Suprock et al. (2006), Suprock and Roth (2006), Roth (2006), and Roth and Pandit (1999). However, these methods were developed by monitoring one specific geometry of endmill. Therefore, the focus of this research is to develop a universal algorithm that is capable of real-time monitoring for impending tool failure when machining with flat, ball, roughing, or tapered endmills.

MATHEMATICAL THEORY

The wear curve generated will be presented as a composition of data transforms applied to tri-axial accelerometer signals sampled at a constant rate. To begin with, the tri-axial data points are windowed into $3 \times n$ matrices:

$$W_i = \begin{bmatrix} x_i, x_{(i+1)}, \dots, x_{(i+n)} \\ y_i, y_{(i+1)}, \dots, y_{(i+n)} \\ z_i, z_{(i+1)}, \dots, z_{(i+n)} \end{bmatrix} \quad (1)$$

and then the rows (corresponding to the x, y, and z sensor directions) are mean subtracted to remove sensor magnitude offsets and zero center the data. Then, through the steps discussed herein, each data window, W_i , is transformed into a real value, R_i , which reflects the cut energy and is used for real time failure forecasting. R_i is obtained from W_i via the following transformations.

The first transform C , vector crossing, maps each window of data, W_i , into a $1 \times n$ vector $H=C(W_i)$:

$$H = [u_i \times \sqrt{(x_i^2 + y_i^2 + z_i^2)}, \dots, u_{(i+n)} \times \sqrt{(x_{(i+n)}^2 + y_{(i+n)}^2 + z_{(i+n)}^2)}] \quad (2)$$

where

$$u_i = \begin{cases} 1 & \text{if } (x_i + y_i + z_i) \geq 0 \\ -1 & \text{if } (x_i + y_i + z_i) < 0 \end{cases}$$

The second transform, A , maps the $1 \times n$ vector H to the vector $S=A(H)$ where S is the autoregressive power spectrum of H . Specifically, an autoregressive (AR) model is fit to the vector H :

$$H(t) = \phi_1 H(t-1) + \dots + \phi_p H(t-p) + a_t \quad (3)$$

where a_t is the model residual.

Rearranging in terms of the residuals, this equation can be written as:

$$H_t = (1 - \phi_1 B - \dots - \phi_p B^p)^{-1} a_t = \sum_{j=0}^t G_t a_{t-j} \quad (4)$$

where,

$$G_j = g_1 \lambda_1^j + \dots + g_p \lambda_p^j \quad \& \quad \lambda^p - \phi_1 \lambda^{p-1} - \dots - \phi_p = 0$$

$$g_i = \frac{\lambda_i^{p-1}}{\prod_{j \neq i} (\lambda_i - \lambda_j)} \quad , \quad i \neq j \quad (5)$$

Using the modal decomposition coefficients:

$$d_i = \sum_{j=1}^p \frac{g_i g_j}{1 - \lambda_i \lambda_j} \sigma_a^2 \quad , \quad i=1, 2, \dots, p \quad (6)$$

the AR power spectrum can be found using:

$$S(\omega) = \frac{\Delta}{2\pi} [d_1 (1 - \lambda_1^2) (1 - \lambda_1 e^{-j\omega\Delta})^{-1} (1 - \lambda_1 e^{j\omega\Delta})^{-1}] \quad (7)$$

$$[+ \dots + d_p (1 - \lambda_p^2) (1 - \lambda_p e^{-j\omega\Delta})^{-1} (1 - \lambda_p e^{j\omega\Delta})^{-1}]$$

where σ_a is the standard deviation of the residuals and $\omega = |\ln(\lambda)/\Delta t|$. Calculating the spectrum, S , from the autoregressive model allows the stochastic portions of the signal to be removed from the estimate, providing a clearer spectral output. For a further description of autoregressive modeling, refer to Pandit (1991).

The third transformation, F , is the Discrete Cosine Transform (DCT); which takes the AR power spectrum, S , back to the time domain. This is done to group the dominant spectral energy of S into the first few coordinates, removing the need to monitor a specific frequency. In particular, $Q=F(S)$ is the vector whose k^{th} coordinate is:

$$Q(\kappa) = \eta_\kappa \sum_{\omega=0}^{0.5(\Delta t)^{-1}} S(\omega) \cos\left\{\frac{(\pi(2\omega)(\kappa))}{(\Delta t)^{-1}}\right\} \quad (8)$$

where

$$\eta_\kappa = \frac{1}{\sqrt{(0.5(\Delta t)^{-1})}} \quad \text{for } \kappa=0$$

$$\eta_\kappa = \sqrt{\left[\frac{2}{(0.5(\Delta t)^{-1})}\right]} \quad \text{for } 1 \leq \kappa \leq 0.5(\Delta t)^{-1}$$

The final transformation of the method, T , extracts the first periodic component of Q . In particular, $R_i=T(Q)$ is the second coordinate (Q_2) of Q .

Note, the second coordinate is utilized since it is the first periodic component of the transform. Since the dominant (toothpass) frequency is of high magnitude and possesses higher energy modes at multiples throughout the frequency

spectrum, this frequency will be the first transfer component after the DC offset of the spectrum, or (Q_2).

In summary, the input, W_i , is mapped through the discussed sequence of transformations into the real values, R_i , according to:

$$R_i = T(F(A(C(W_i)))) \quad (9)$$

Once obtained, the value R_i is appended to the historical values of $P=(R_1, R_2, \dots, R_i)$ and used to statistically track the condition of the tool. After appending the value R_i , the entire vector P is given a linear fit in a least squares sense. This fit will take the form of a 1st order slope intercept:

$$P(i) = m_i t_i + b_i \quad (10)$$

where t_i is the time index of the value R_i .

A linear fit is given to P since the tool should wear in a linear fashion until the tool approaches failure, at which point the wear increases exponentially (shown later in Figure 2). For this reason, when a linear fit no longer provides an adequate forward estimate of the tool's state, it is an indication that failure is approaching.

After computing the linear coefficients shown in Equation 10, the prediction of the future state, $\hat{P}(i+1)$, can be calculated as:

$$\hat{P}(i+1) = m_i t_{(i+1)} + b_i \quad (11)$$

Simultaneously, the standard deviation of the vector P is used in order to define a 99% upper confidence interval for $\hat{P}(i+1)$ from the vector P based on the following relationship:

$$U(i+1) = \hat{P}(i+1) + 2.576 \times \left(\frac{1}{i} \sum_{r=1}^i [P(r) - \bar{P}(r)]^2 \right)^{0.5} \quad (12)$$

where 2.576 is the z-score coefficient for the standard deviation at 99% confidence, and where $U(i+1)$ is the upper confidence threshold. This relationship assumes a large set of statistically normal (in a Gaussian sense) values centered around the forecast value $\hat{P}(i+1)$ given by evaluating Equation 11.

Once the future state $P(i+1)$ is realized by the system, the predicted value is compared

to the confidence bound given by Equation 12:

$$\delta_1 = U(i+1) - P(i+1) \quad (13)$$

If δ_1 is a negative value, the forecast confidence threshold has been exceeded by the realized system value $P(i+1)$. This is identified as a failure cue (discussed in the Method Application section). Upon entering a failure cue, the forecast is recalculated as:

$$P(i+2) = m_i(i+2) t_{(i+2)} + b_i \quad (14)$$

Likewise, the 99% upper confidence interval is then also recalculated as:

$$U(i+2) = (\hat{P}(i+2)) + 2.576 \times \left(\frac{1}{i} \sum_{r=1}^i [P(r) - \bar{P}(r)]^2 \right)^{0.5} \quad (15)$$

Once the second future state $P(i+2)$ is realized by the system, the predicted value is once again contrasted against the second forward confidence bound given by Equation 15:

$$\delta_2 = U(i+2) - P(i+2) \quad (16)$$

If δ_2 is also a negative value, the forecast confidence threshold has also been exceeded by the realized system value $P(i+2)$. This event is noted as a failure mode. In the case that δ_2 is a positive value, the failure is considered false and the entry $P(i+1)$ is discarded as an outlier. In this case, the value $P(i+1)$ is not included in future calculations of confidence. Two consecutive outliers are necessary to indicate an approaching failure since the statistical probability of two outliers occurring sequentially in a small population of samples is extremely low. Additionally, it is unlikely that extraneous events (rogue chips, material hard spots, etc.) would endure over multiple data windows. Therefore, two consecutive outliers provide a good prognosis that there has been a statistical change in the tool's condition that is causing it to exceed the confidence threshold.

EXPERIMENTAL PARAMETERS

During this series of wear tests, the tri-axial accelerometer data were collected from linear passes through 4340 series tool steel. Data were captured as 32768 datapoints per pass

which corresponds to 10.92 seconds. The tri-axial accelerometer data were captured at the simultaneous DAQ rate of 3000 Hz. Figure 1 describes the orientation of the accelerometer axes with respect to the cut feed. Tri-axial accelerometer data is used since all three axes contribute to a greater system resolution and thus, better failure forecasts than possible with only a single sensor axis.

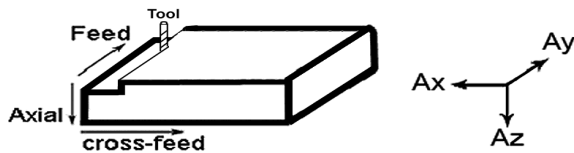


FIGURE 1. STRAIGHT PASS TOOL ORIENTATION.

The spindle speed was kept constant over all wear tests in order to enhance the repeatability through similar drive dynamics. Similarly, the axial cut depth was maintained at 12.7 mm for all of the tests. This was done in order to create a consistent bending moment dynamic on the spindle. However, the feed rate was adjusted in order to keep a consistent linear advance per toothpass (i.e. the feed rate for the 4 flute tools was 375.76 mm/min whereas the feed rate for the 3 flute tools was $\frac{3}{4}$ of the 4 flute rate at 281.82 mm/min). The ball nose and tapered tools were composed of HSS while the roughing tools were cobalt alloy M42. Both tapered tools had a 7° taper angle. The tools utilized in this set of experiments were selected from random domestic and international manufacturers in order to ensure that the observed wear curves are not a function of a particular manufacturing process. For all of the tools tested, surface “burning” occurred prior to flute/shank fracture, edge burring, or the tool no longer cutting within tolerance. Therefore, tool failure was defined by the onset of this surface burn.

A 100th order autoregressive model is fit to each windowed dataset of 32768 data points. This model order was chosen since previous studies have shown that a 100th order model is sufficient to provide a high enough resolution of the frequencies present in a typical endmilling system. Furthermore, a constant order is used to model all of the data windows since this reduces computational burden. The method described in this work is able to achieve on-line (real time) condition monitoring, only requiring a processing time of 1.86 seconds per dataset which is more than sufficient when contrasted with the dataset length of 10.92 seconds.

With these parameters, it is shown that the algorithm produces similar trends capable of forecasting impending tool failure, regardless of geometry in all cases without requiring alterations or a priori information regarding the specific cutting geometry being analyzed. In addition, the application of AR modeling and primary component analysis by the Fourier inverse was shown successful by the authors Suprock et al. (2006) while using similar parameters. The application of this method begins by sampling multi-channel 3000 Hz DAQ data at a chosen step size.

In order to zero-center the datasets, the input channels are mean subtracted before processing. Each data window is then processed as detailed in equations 1 through 8. The output trends are then independently processed by the statistical confidence procedure described in equations 9 through 16. If a realized future state exceeds the confidence projection of the system, a failure cue is indicated. A failure cue is a single magnitude which has exceeded the statistical threshold for realistic future values. If a failure cue occurs, the statistical confidence algorithm forecasts a value two steps ahead of the current state and compares the confidence threshold of this new forecast to the corresponding future state. If the future state of the wear curve exceeds the forecast confidence for a second data window, the system is considered to be approaching a failure mode. For this reason, two consecutive outliers are necessary for the declaration of a failure mode.

RESULTS

Previous investigations regarding wear behavior of cutting tools have established a schematic for the progression of wear throughout the useful life. Figure 2 shows the theoretical wear behavior expected in flat endmill tools.

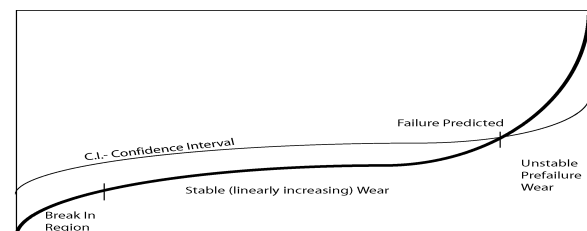


FIGURE 2. KNOWN WEAR CURVE FOR FLAT ENDMILL TOOLS

As will be seen, applying the algorithm to the tri-axial accelerometer life test data collected from the various geometry tools produces wear trends similar to those found in Figure 2. Furthermore, these trends will be shown to be capable of reliably tracking the condition of the tool and forecasting impending tool failure. In this paper, failure is defined as the onset of a surface burn. Recall, surface burning occurred prior to flute/shank fracture, edge burring, or the tool no longer cutting within tolerance for all wear tests.

As will be observed for all of the all tests performed, the algorithm consistently produced both interpretable wear trends and reliable failure prognoses. Due to the highly congruent results of both wear tests and failure prognoses, each tool geometry type will be presented separately and then compared. The wear trends shown in Figures 3-10 use vertical lines to represent the monitoring index P and a solid trend line to represent the confidence threshold U .

Wear Tests of Flat Endmill Tools

As previously mentioned, two flat endmilling life tests were completed and analyzed to demonstrate the general capabilities of the technique. The results of applying the technique to these two tests can be found in Figures 3 and 4. As shown, the trends developed for both of these tools, prior to the tool's failure, are relatively stable. The observed stability of the datasets can be attributed to the nature of both the autoregressive modeling and the holistic representation of spectra made possible by the real Fourier inverse.

Figures 3 and 4 show that, as in previous investigation of flat endmilling tools by Suprock et al. (2006), the autoregressive model coupled, with the real Fourier inverse, is able to effectively remove noise from the system, thereby providing a clear observation of the flat endmilling tool's toothpass frequency. Moreover, as the tool wears, it is apparent that the trends output by the algorithm, when applied to the two life tests, are very comparable to those of the theoretical wear curve in Figure 2. More specifically, the magnitude of the acceleration signal is found to increase rapidly once the system becomes unstable.

In addition, as this wear curve magnitude grows over the sample sets, the indexes intersects the confidence threshold. When the algorithm output curve exceeds this threshold for two consecutive datasets, tool failure is predicted. To this end, during the initial system stability, the confidence interval is seen to closely follow the data magnitude. This initially stable relationship allows the confidence interval to rapidly identify, the onset of increasing acceleration activity associated with an approaching failure mode. For both tools, the prediction of impending tool failure is identified by the algorithm roughly 4.8 cm of cut distance before the actual failure event occurs.

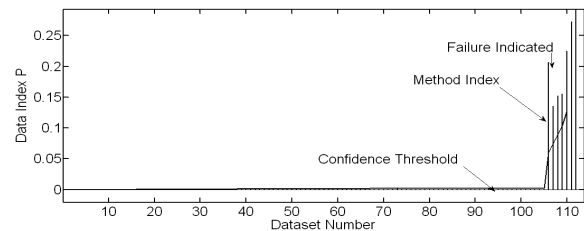


FIGURE 3. FLAT 1 RESULTS.

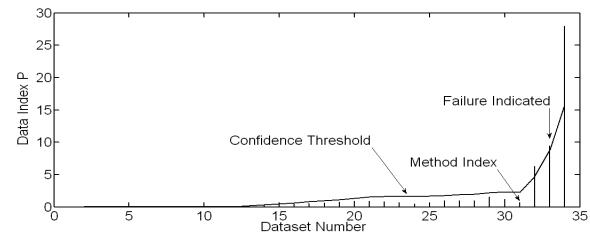


FIGURE 4. FLAT 2 RESULTS.

Wear Tests of Ball Nose Endmill Tools

As was true with the two flat endmilling tool life tests, the two ball nose wear trends developed from the life tests are presented along with the respective 99% confidence threshold (refer to Figures 5 and 6). By comparing the ball nose endmilling trends in Figures 5 and 6 to the flat endmilling trends in Figures 3 and 4, it can be seen that significant similarities exist between the algorithm's trends for both endmill geometries.

Specifically, the ball nose life test results are also found to initially exhibit a highly stable tool wear curve with close confidence. However, as the tool wears, there is an increasing level of deviant activity as the tools approach failure. The fact that the generated trends show minimal

noise before failure is approached indicates that the algorithm is successfully removing the noise from the system and correctly identifying features indicative of a deteriorating tool. The algorithm is effective for both ball nose tests with a forecast made at 23.1 and 6.1 cm of cut distance before realization of a failure mode.

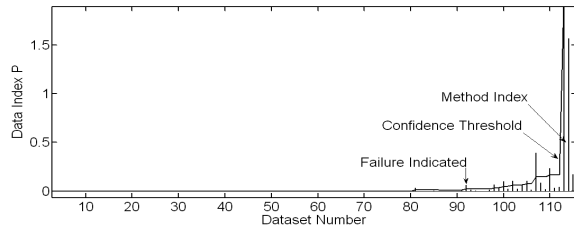


FIGURE 5. BALL NOSE 1 RESULTS.

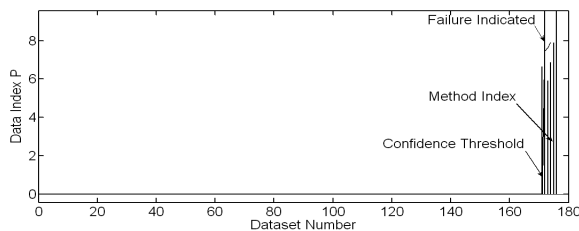


FIGURE 6. BALL NOSE 2 RESULTS.

Wear Tests of Tapered Endmill Tools

As presented previously with both the flat and ball nose life tests, the results of the tapered endmill tests are presented with the algorithm's wear trend outcomes. Also, similar to the previously discussed life test results, the upper confidence threshold is presented. This curve once again closely follows the wear curve during the stable wear period and the algorithm is reliable for both tapered life tests, producing failure forecasts at 2.75 and 6.4 cm of cut distance before the tool fails.

As can be seen in Figures 7 and 8, the wear behavior of tapered endmills is highly similar to the wear behavior exhibited by both flat and ball nose tools. Like the ball nose tests, the algorithm is shown to correctly identify an impending failure without a priori knowledge about the tool geometry. Due to wear trend similarity between the tapered, ball nose, and flat tool life tests, the statistical monitoring algorithm once again does not require alteration.

Clearly the algorithm successfully tracks the wear behavior over the duration of the tapered tests and the toothpass energy can be seen to

significantly increase as the tool approaches failure. In tapered tests 1 and 2, the algorithm is shown to be successful for two distinct types of failure, flute deterioration and normal wear.

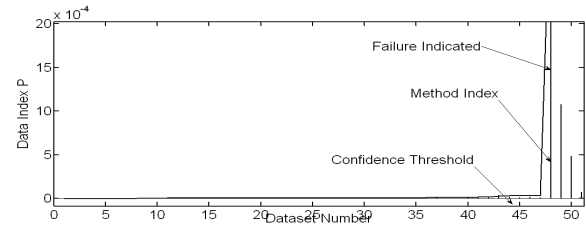


FIGURE 7. TAPERED 1 RESULTS.

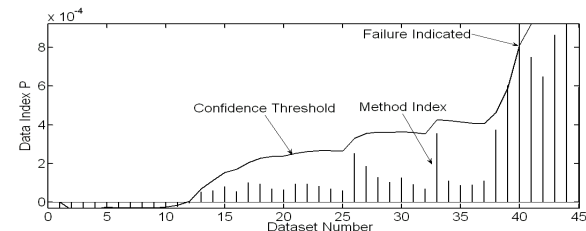


FIGURE 8. TAPERED 2 RESULTS

Wear Tests of Roughing Endmill Tools

The roughing endmill is the final tool geometry investigated. As in the previous three tool geometry life tests, both 99% upper statistical confidence and wear trend results are presented. The algorithm is effective for both of the roughing endmill life tests, producing failure forecasts at 8.54 and 9.74 cm of cut distance before the tool fails. It is found that roughing tools produce considerably more noise close to the tool toothpass frequency. Thus, the benefits of employing an autoregressive model were clearly evident for these tools. The ability to generate a spectrum from an approximate model is critical to excluding noise that could affect the reliability of analysis. Figures 9 and 10 present the results of the roughing tool wear tests.

As can be seen in Figures 9 and 10, the wear curves for roughing endmills are congruent with flat, ball nose, and tapered tool geometries. Although the life tests show slightly higher variability for the roughing tools due to their geometry, the wear curves are clear and provide substantial failure prediction ability. Furthermore, in addition to the generation of usable wear curves, the algorithm also successfully identifies and discards a singular outlier during roughing life test 2 (Figure 10).

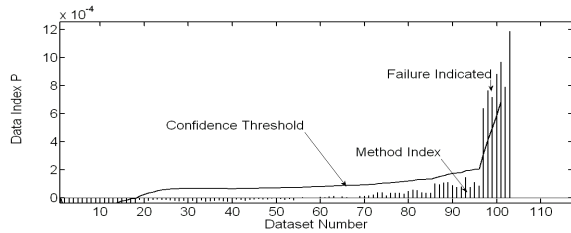


FIGURE 9. ROUGHING 1 RESULTS

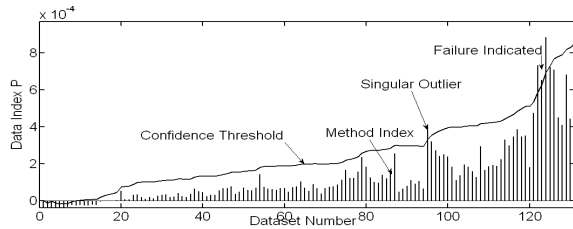


FIGURE 10. ROUGHING 2 RESULTS.

Discussion of Wear Trends and Tool Condition Monitoring

As shown in all of the endmill tool geometries tested, there is a high similarity in the wear curves generated by the technique. This can be seen by contrasting the curves shown in Figure 3-10. Furthermore, these curves clearly track the condition of the tool and are similar in nature to the theoretical wear curve (shown in Figure 2). Additionally, the similarities observed in the wear trends allow the algorithm to make reliable failure forecasts without a prior knowledge of the tool geometry.

Consistent results have been demonstrated using this method for the generation of wear curves and failure forecasting. The stability of these trends is attributed to the use of the autoregressive model to reduce noise. Additionally, the use of a real Fourier inverse of the autoregressive spectrum provides a more holistic observation of the spectrum than a specific frequency band and does not require a priori knowledge of the cutting parameters.

As shown, the algorithm demonstrates success in all of the tests conducted. Table 1 outlines the linear cut distance remaining between the impending failure forecast and deterioration of the tool. As previously mentioned, for these investigations, surface burning occurred prior to flute/shank fracture, edge burring, or the tool no longer cutting within tolerance for all of the wear tests conducted. Furthermore, impending failure for the tool is

established by the technique when the confidence interval threshold is exceeded twice consecutively and that tool failure is defined as the onset of a surface burn. The predictive distances presented in Table 1 represent the linear cut distance between these two events.

TABLE 1. CUT DISTANCE BETWEEN PREDICTION AND FAILURE.

	Distance (cm)
Flat 1	4.87
Flat 2	4.80
Ball 1	23.10
Ball 2	6.10
Tapered 1	2.75
Tapered 2	6.40
Rough 1	8.54
Rough 2	9.74

CONCLUSIONS

It is evident from the outcome of these tests that there is a high level of congruence between wear curve trends of Flat endmilling tools the ball nose, tapered, and roughing tool types. Additionally, the algorithm is shown to produce wear trends for all geometries from which statistical failure forecasting is implemented. The stability of the produced wear curves is evidence that model based noise reduction is a valuable method for tracking activity at the tool toothpass frequency. Through this study, it is also found that Roughing endmill tools produce high levels of noise at the toothpass frequency, although it is not beyond the filtering capability of an AR model.

In this work, the research objective of producing wear curves for use in a tool condition monitoring application has been successfully achieved. The method investigated is able to correctly identify wear trends that are usable for effective on-line (real time) tool condition monitoring in all cases for all tool geometries. Furthermore, the endmilling tool condition monitoring algorithm developed in this work is effective at monitoring the condition of the cutting tool and forecasting failure without a priori knowledge of the tool's toothpass frequency, flute configuration, or tool geometry.

REFERENCES

Azeem, A., H. Feng, and L. Wang, (2003), "A simplified approach for determining empirical cutting force coefficients for Ball-End Milling," *Transactions of the North Amer. Manuf. Research Inst. of SME*, Vol. 31, pp. 121-128.

Chen, J. C., and J. C. Chen, (2005), "An artificial neural networks-based in-process tool wear prediction system in milling operations," *The International Journal of Advanced Manufacturing Technology*, Vol 25. 5- 6, pp. 427-434.

Choi, Y., and S. Chung, (2006), "Monitoring of Micro-Drill Wear by Using the Machine Vision System," *Transactions of the North Amer. Manuf. Research Inst. of SME*, Vol. 34, pp. 143-150.

Ko, J. H., and D. W. Cho, (2002) "Accurate 3D Cutting Force Prediction Using Cutting-Condition-Independent Coefficients in Ball-End Milling," *Transactions of the North Amer. Manuf. Research Inst. of SME*, Vol. 30, pp. 223-230.

Ning, L., and S. C. Veldhuis, (2004), "Mechanistic Modeling of Ball End Milling Including Tool Wear," *Transactions of the North Amer. Manuf. Research Inst. of SME*, Vol. 32, pp. 103-110.

Olortegui-Yume, J.A., and P. Y. Kwon, (2006), "Tool Wear Evolution in Multilayer Coated Inserts Using Topographic Imaging," *Transactions of the North Amer. Manuf. Research Inst. of SME*, Vol. 34, pp. 143-150.

Pandit, S.M., (1991), *Modal and Spectrum Analysis: Data Dependent Systems in State Space*, John Wiley & Sons, Inc., New York.

Rodriguez, C., and T. Altan, (2000), "Effect of process parameters upon tool wear of Ball-Nose end mills," *Transactions of the North Amer. Manuf. Research Inst. of SME*, Vol. 28, pp. 221-226.

Roth, J.T., (2006), "Using the Eigenvalues of Multivariate Spectral Matrices to Achieve Cutting Direction and Sensor Orientation Independence," *Trans. of the ASME, J. of Manuf. Sci. and Engr.*, Vol. 128, pp. 350-354.

Roth, J. T., and S. M. Pandit , (1999), "Using

Multivariate Models to Monitor End-Mill Wear and Predict Tool Failure," *Technical Papers of the North Amer. Manuf. Research Inst. of SME*, Vol. 27, pp. 63-68.

Suprock, C., J. Piazza, and J. T. Roth, (2006), "Directionally Independent Failure Prediction of End-milling Tools during Pocketing Maneuvers," *ASME International Conference on Mfg. Science and Engr.*, MSEC2006-21089, 10 pp.

Suprock, C., and J. T. Roth, (2006), "Directionally Independent Failure Prediction of End Mill Cutting Tools: An Investigation of Noise Reduction Using Higher Dimensional Real Fourier Analysis," *ASME International Mechanical Engineering Congress and Exposition*, IMECE2006-14968, 10 pp.

Xu, M., C. K. Schuyler, B. K. Fussell, and R. B. Jerard, (2006), "Experimental Evaluation of a smart machining System for Feedrate Selection and Tool Condition Monitoring," *Transactions of the North Amer. Manuf. Research Inst. of SME*, Vol. 34, pp. 151-158.